This article has been accepted for publication in a future issue of this journal, but has not been fully edited. Content may change prior to final publication. Citation information: DOI 10.1109/TSTE.2018.2841018, IEEE Transactions on Sustainable Energy

Reconfigurable Control for Fault-Tolerant of Parallel Converters in PMSG Wind Energy Conversion System

Gen Chen, *Student Member, IEEE*, and Xu Cai

***Abstract*—Offshore wind energy conversion system (WECS) usually adopts parallel converters to expand power capacity and improve reliability because of limited power rating of power devices, harsh marine environment, and poor maintenance accessibility. Any faulty converter is cut off under traditional fault-tolerant control. When all parallel converters are faulty, the wind turbine must be shut down. Although simple, such a fault-tolerant control reduces system availability. Thus, a reconfigurable control for fault-tolerant of parallel wind power converters is proposed in this paper. The current reference of every phase leg in parallel converter system is reconfigured post-fault according to their healthy states. The proposed reconfigurable control is realized in software level and without requiring redundant hardware. Compared with traditional fault-tolerant control, the proposed reconfigurable control only cuts off the faulty legs rather than faulty converter, and makes full use of all healthy legs. The reconfigurable control improves the availability of parallel wind power converters and provides multiple-leg fault ride-through capability to WECS, enhancing reliability and electricity generation. The simulation and experimental results validate the feasibility and effectiveness of the proposed reconfigurable control.**

***Index Terms*--Reconfigurable control, fault tolerant, parallel wind power converters, permanent magnet synchronous generator, wind energy conversion system.**

I. Introduction

RENEWABLE energy, particularly wind power and photovoltaic sources, is undergoing remarkable improvement worldwide. This advancement stems from the essential demand for global sustainable development. Installed wind capacity is growing rapidly, and the capacity of single wind turbine is increasing steadily [1,2]. With the development of land wind resource, the focus is shifting toward offshore wind resource for its great advantages, such as stable wind speed, low environmental impact, and close location to consumers [3,4]. According to the types of generators equipped with wind turbine, the configuration of the wind energy conversion system (WECS) can be divided into three categories, namely, doubly fed induction generator (DFIG) with partial-scale power converter, asynchronous induction generator (IG) with full-scale power converter, and permanent magnet synchronous generator (PMSG) with full-scale power converter. The rated power of state-of-the-art WECS has been steadily increasing and currently approaching 10 MW, which exceeds that of a single converter because of the limited power rating of power semiconductor. Therefore, power converters in parallel configuration are widely adopted in high power DFIG- [5,6] and PMSG-based [7,8] WECS. Increasing wind power penetration results in strict grid codes, and the increasing capacity of wind turbine and strict grid codes push WECS toward full-scale power conversion [9]. The PMSG is the most promising technology for high-power generator in terms of efficiency [10]. In addition, the direct-drive PMSG WECS exhibits high reliability by eliminating gearbox [11]. The PMSG WECS will be the dominant configuration in future, especially for offshore wind turbine.

Considering that offshore WECS is expensive to install, operate, and maintain, the reliability of offshore WECS is a critical issue. As an essential part of WECS, the performance of a wind power converter bears significant effects on the system reliability [12]. Field survey data indicate that power converter is the most fragile part of WECS [13,14]. In the parallel system, the circulating current between parallel converters is inevitable, and control strategies for suppressing the circulating current are investigated in depth [15,16]. Reliability can be improved by reliability-oriented topology and control strategies. The N+X parallel configuration of converters can improve system reliability by redundancy backup [17]. The parallel operation of multiple power converters can improve reliability of WECS. In addition, numerous studies focus on strategies to improve the reliability of the converter. Reducing and smoothing thermal stress is key to improve reliability [18-21], because this stress is the main failure factor of power devices. The optimized modulation [19], optimized reactive power flow [20], and improved power electronics model [21] are introduced to reduce thermal stresses. However, these reliability-improved controls are only suitable pre-fault but invalidated post-fault.

Therefore, fault-tolerant control is attractive with increasing demand of reliability in high-power field. Fault-tolerant control is always realized on the basis of hardware redundancy. Based on the type of hardware redundancy, these

This work was supported in part by the National Key Research and Development Program of China under Grant 2016YFB0900901, and in part by the National Nature Science Foundation of China under Grant 51507101. (*Corresponding author: Xu Cai*).

The authors are with the Department of Electrical Engineering, Shanghai Jiao Tong University, Shanghai 200240, China (e-mail: chengen@sjtu.edu.cn; xucai@sjtu.edu.cn).

This article has been accepted for publication in a future issue of this journal, but has not been fully edited. Content may change prior to final publication. Citation information: DOI 10.1109/TSTE.2018.2841018, IEEE Transactions on Sustainable Energy

methods are classified into four categories, namely, switch-, leg-, module-, and system-level [22]. When fault happens, the faulty switch, leg and module are replaced by redundant ones. In addition, the faulty leg can be connected to the midpoint of dc-link by additional triacs to maintain continuous operations. These remedial actions typically contain hardware and software reconfigurations that extend normal operations or a derating system that prevents unexpected shutdowns [23-26]. In [27], three open-circuit fault-tolerant control strategies are presented, namely, normal channel direct compensation, normal channel asymmetric currents compensation, and equivalent current value compensation. These fault-tolerant control strategies provide smooth torque and reduce stator copper losses. In [28], an asymmetric current injection based open-circuit fault-tolerant control is proposed for PMSM drive. An exact d-axis current injection fault-tolerant control is proposed for outer switch open-switch fault in three-level rectifier [29] because the rectifier and inverter have different current loops. Parallel converters are switched from two three-leg modes into a five-leg mode by a fault-tolerant bridge to ride through a single-phase fault [30].

Reconfigurable fault-control is an emerging research hotspot [31-33]. In [31], the three-phase current references are reconfigured under open-circuit fault of current sensor. In [32], a carrier-based reconfiguration method was proposed for the three-level NPC inverter. The duty cycles of the outer and inner switches are modified post-fault. The back-to-back converters are reconfigured to a five-leg converter that shares a leg by additional bidirectional switches [33]. However, these reconfigurable control strategies only deal with a single fault. In a parallel converter system, faults may occur in multiple legs, such as fault in different converters at different phases. However, multi-fault ride through reconfigurable control strategy is scarce.

A reconfigurable control for fault-tolerant of parallel wind power converters in PMSG WECS is proposed in this paper. The current reference of every phase leg in the parallel converter system is reconfigured post-fault according to their healthy states. The proposed reconfigurable control is realized in software level and no redundant hardware is required. Compared with traditional fault-tolerant control, the proposed reconfigurable control only cuts off the faulty legs rather than the faulty converter, making full use of all healthy legs. The reconfigurable control improves the availability of parallel wind power converters and provides multiple-leg fault ride-through capability to WECS, enhancing its reliability and electricity generation. The simulation and experimental results validate the feasibility and effectiveness of the proposed reconfigurable control.

The rest of this paper is organized as follows. The reconfiguration and constrains of parallel converter system are presented in section II. The fault detection and isolation methods are presented in section III. The proposed reconfigurable control is described in detail in section IV. The simulation and experimental results validate the feasibility and effectiveness of the proposed reconfigurable control in sections V and VI, respectively. Several conclusions are summarized in section VII.

II. Reconfiguration and Constrains of Parallel Converter System

A WECS based on PMSG is considered, and Fig. 1 illustrates its system configuration. The WECS consists of the wind turbine, PMSG, power converter, and step-up transformer. The PMSG is directly driven by the wind turbine. The wind power converter adopts parallel configuration with converters of two-level topology sharing a common dc bus. The fault reconfigurable parallel wind power converters are highlighted in Fig. 1 by the pink-dashed block diagram.

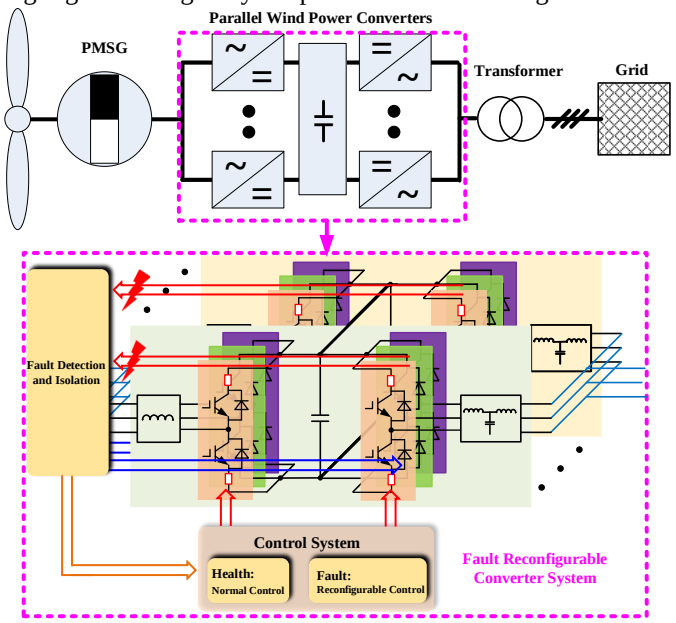

Fig. 1. Fault reconfigurable parallel converter system in PMSG WECS

The fault reconfiguration power converter system consists of back-to-back converter, control system, and fault detection and isolation module. The fault detection and isolation module is the most essential part of the system. The control system adopts normal and reconfigurable controls according to the healthy and faulty states of converters, respectively. The overall performance of the reconfigurable control is closely related to the speed and accuracy of fault detection and control strategy.

A. Fault types and reconfiguration method

Faulty legs are cut off and isolated post-fault, whereas healthy ones remain operating.

The fault type of parallel converters system is defined as $F_{i\text{-}jt}$, where i denotes the number of faulty converters, i=1,2,⋯,N. j denotes the number of faulty legs, j=i, i+1,⋯, 3*i. t distinguishes the phases of faulty legs, whereby in t=s, faulty legs are at the same phase, and t=d, faulty legs are at different phases.

A parallel system with two converters is considered to simplify the analysis. The fault types and reconfiguration method are described in detail.

In $F_{1\text{-}jd}$(j=1,2,3), $F_{1\text{-}1d}$ with fault in leg A_1 is considered, as shown in Fig. 2(a). Leg A_1 is cut off post-fault, and legs B_1 and C_1 remain working. The parallel converter system is

This article has been accepted for publication in a future issue of this journal, but has not been fully edited. Content may change prior to final publication. Citation information: DOI 10.1109/TSTE.2018.2841018, IEEE Transactions on Sustainable Energy

reconfigured and highlighted by the blue solid block diagram.

In $F_{2\text{-}2d}$, faults in legs A_1 and B_2 are considered, as shown in Fig. 2(*b*). Legs A_1 and B_2 are cut off post-fault. Legs A_2, B_1, C_1, and C_2 are reconfigured and highlighted by the blue solid block diagram. $F_{2\text{-}2s}$, with faults in legs A_1 and A_2 are considered, as shown in Fig. 2(*c*). Under this condition, the system cannot be reconfigured because of the absence of healthy leg in phase A, which is highlighted by the blue-dashed block diagram.

In $F_{2\text{-}3t}$, the parallel system can be reconfigured when three faulty legs are at different phases. $F_{2\text{-}3d}$, with fault in leg A_1 is considered, as well as C_1 and B_2, as shown in Fig. 2(*d*). Legs A_1, C_1, and B_2 are cut off post-fault. Legs A_2, B_1, and C_2 are reconfigured and highlighted by the blue solid block diagram. The parallel system cannot be reconfigured under $F_{2\text{-}3s}$. For example, faults in legs A_1, C_1, and A_2, as shown in Fig. 2(*e*), are highlighted by the blue-dashed block diagram.

When more than four legs are faulty, faulty legs at the same phase are present. Thus, the parallel system cannot be reconfigured. For example, $F_{2\text{-}4s}$, faults in legs A_1, C_1, A_2 and B_2, as shown in Fig. 2(*f*), are highlighted by the blue-dashed block diagram.

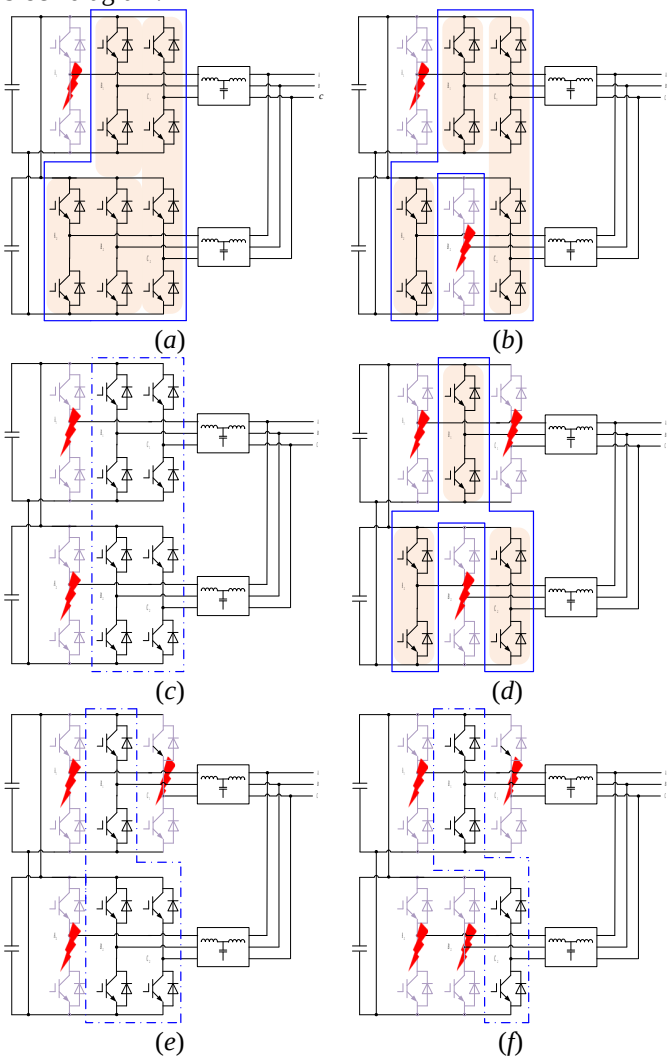

Fig. 2. Fault types and reconfiguration methods of parallel power converters

B. Reconfiguration constraints of N parallel converters

The reconfiguration constraints of N parallel converters can be summarized according to the analysis of the above section. The number of faulty legs in each phase is defined as $n_{kF}(k=a,b,c)$, and the number of healthy legs in each phase is defined as n_{kH}, where $0 \le n_{kF} \le N$, $n_{kH} = N - n_{kF}$.

The post-fault reconfigurable constraints of N parallel converters are as follows:

$$\min\{n_{kH}(k=a,b,c)\} \ge 1 \tag{1}$$

From (1), as long as one healthy leg is present in every phase, the parallel power converter system can be reconfigured post-fault.

The rated power of post-fault reconfigured converter is as follows:

$$P_r = \min\{n_{aH}, n_{bH}, n_{cH}\} * P \tag{2}$$

where P is the rated power of a single converter.

III. Fault Detection and Isolation

A. Fault detection

Fault detection is essential part to the fault reconfigurable system. Fault detection is realized by analyzing the state signals of the device to determine whether its operation is normal or not. Many methods are available for fault detection, such as monitoring voltage and current [34-37]. The fault detection method proposed in [34] is adopted in this paper. The open-circuit fault of phase leg is detected by comparing the measured and estimated values of the phase voltage. Although this fault detection method is simple, additional sensors are required. The switching function model-based sensorless fault diagnostic method [37] is an alternative.

Fig. 3 shows a phase leg of a power converter. The measured phase voltage and estimated values are u_{knm} ($k=a,b,c$) and u_{kne}, respectively. The estimated phase voltage is as follows:

$$u_{kne} = (2S_k - 1)\frac{V_{dc}}{2} \tag{3}$$

where S_k is the switching state function of phase leg. When S_k =1, the upper IGBT turns on and the lower one turns off. By contrast, the upper IGBT turns off and the lower one turns on when S_k =0.

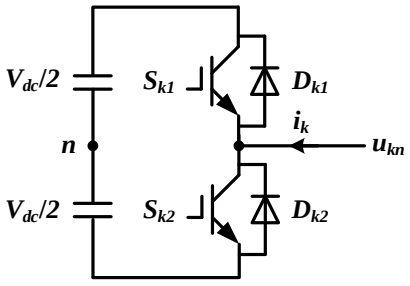

Fig. 3. One phase leg of power converter

The voltage error between the measured phase voltage and

This article has been accepted for publication in a future issue of this journal, but has not been fully edited. Content may change prior to final publication. Citation information: DOI 10.1109/TSTE.2018.2841018, IEEE Transactions on Sustainable Energy

estimated one is as follows:

$$e_{kn} = u_{knm} - u_{kne} \tag{4}$$

If the power devices ideally switch, the measured phase voltage equals the estimated one under normal operation. Thus, e_{kn}=0. However, due to measurement error, discretizing error, and non-ideal switching characteristics of power devices, such as switching delay and dead time of driver, the voltage error is not zero even under normal operation. Voltage and time criteria are introduced to compensate false fault detection effects to avoid false fault detection.

Voltage criterion is aimed at eliminating measurement and discretizing errors. In voltage criterion, the voltage threshold "h" is introduced, where h=10 V. The voltage error is recognized when $e_{kn}>h$. Time criterion is applied to compensate delay affection caused by control and switching delay. Proper time threshold T is set, which can be calculated by an up-counter. The time threshold T is set as a switching period. $T = N_T T_s$, and system sample time T_s=10 μs. When the switching frequency is 2 kHz, N_T=50. When $n>N_T$, the fault is detected.

Fig. 4 shows the fault detection scheme. The absolute value of the voltage error between measured and estimated voltage is compared with threshold h. If $e_{kn}>h$, then the up-counter starts counting. If $e_{kn}<h$, then the up-counter is reset. When $n>N_T$, the fault is detected.

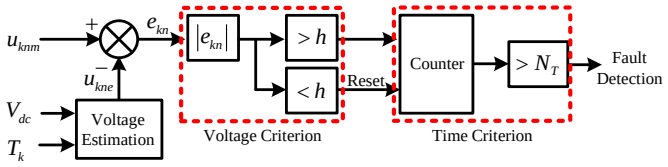

Fig. 4. Fault detection scheme

The open-circuit fault detection time is related to the current direction. In Fig. 3, S_{k1} is with an open-circuit fault. When $i_k>0$, current flows through D_{k1}. Such a fault cannot be detected until the current turns negative and flows through the faulty switch. When $i_k<0$, current flows through S_{k1} and the fault can be detected right now as faulty current flows through the faulty switch.

B. Fault isolation

The open-circuit fault can be isolated by shutting down the driving signals of the faulty legs.

Regarding short-circuit fault, if the fuse acting time is shorter than fault detection time, then the short-circuit fault is diagnosed as open-circuit. With proper choice of fuse cleaning time, the short-circuit fault can be turned into open-circuit one. Therefore, reconfiguration control for open-circuit fault is addressed in this paper.

IV. Reconfigurable Control for Parallel Converter System

A. Reconfiguration of current reference

The healthy state function of phase leg k of jth converter is defined as H_{kj} (k=a,b,c).

$$H_{kj} = \begin{cases} 1 & \text{health} \\ 0 & \text{fault} \end{cases} \tag{5}$$

The limitation of the d-axis current is determined by its healthy states of phase legs.

$$i^*_{d\lim} = \begin{cases} N * I_{\max} & \text{health} \\ \min\{n_{aH}, n_{bH}, n_{cH}\} * I_{\max} & \text{fault} \end{cases} \tag{6}$$

where $I_{\max}$ is the maximum current of a single converter.

The key of the proposed reconfigurable control is the reconfiguration of current references at every phase leg in the parallel converter system. The current references of phase legs are reconfigured according to their healthy state functions. The currents of the phase legs are controlled separately in a three-phase stationary frame, which adjusts to normal and faulty conditions.

The total current reference of each phase is i^*_k, and the current reference for each phase leg in jth converter is i^*_{kj}.

$$i^*_{kj} = \frac{H_{kj}}{\sum_{j=1}^{N} H_{kj}} i^*_k \tag{7}$$

A parallel system with three converters is considered to simplify the analysis of reconfiguration of current references. The current references for phase leg k(k=a,b,c) of converters 1, 2, and 3 are given in (8).

$$i^*_{ki} = \frac{H_{kj}}{\sum_{j=1}^{3} H_{kj}} i^*_k (i = 1,2,3) \tag{8}$$

Fig. 5 shows the reconfiguration scheme of current references. The PI regulator of the outer voltage loop outputs the total d-axis current reference i^*_d. The total current references in three-phase stationary frame are calculated by inverse park transform. The current references for phase legs of converters 1, 2, and 3 can be obtained by (8).

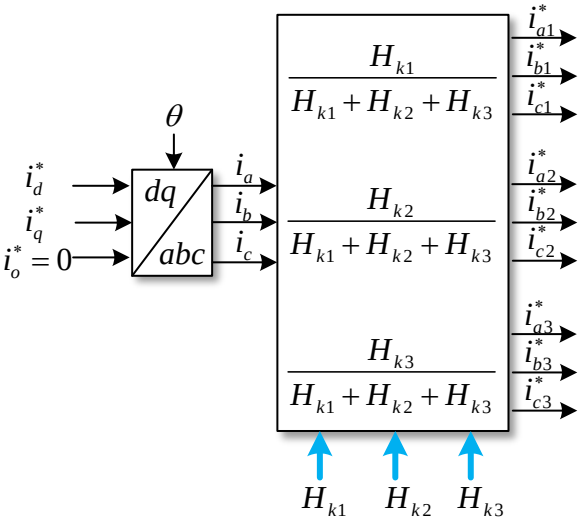

Fig. 5 Reconfiguration of current references

This article has been accepted for publication in a future issue of this journal, but has not been fully edited. Content may change prior to final publication. Citation information: DOI 10.1109/TSTE.2018.2841018, IEEE Transactions on Sustainable Energy

B. Reconfigurable control for fault-tolerant

A parallel system with two converters is considered to present the proposed reconfigurable control strategy in detail.

Fig. 6 shows the control scheme of the proposed reconfigurable control strategy for parallel wind power converters. The inner current loop adopts a PR controller in the three-phase stationary frame. The PI regulator of the outer voltage loop outputs the *d* axis current. Then, the output d-axis current is transformed to current references in the three-phase stationary frame. The current reference of each converter is obtained according to the healthy state function of the phase leg. The PR controller can well track periodic signals in a stationary frame [38], which has infinite gains at reference frequency. Thus, a PR controller in a stationary frame is adopted to track the reconfigured alternating references. The sinusoidal pulse width modulation is adopted. As the currents of legs in the same phase are controlled to the same reference value separately and accurately, the circulating current can be eliminated. Although distinct control strategies are applied for generator and grid sides, the reconfigurable control scheme is similar in the current reference reconfiguration of inner current loops. Therefore, the reconfigurable control strategy for a generator side converter can be obtained similarly.

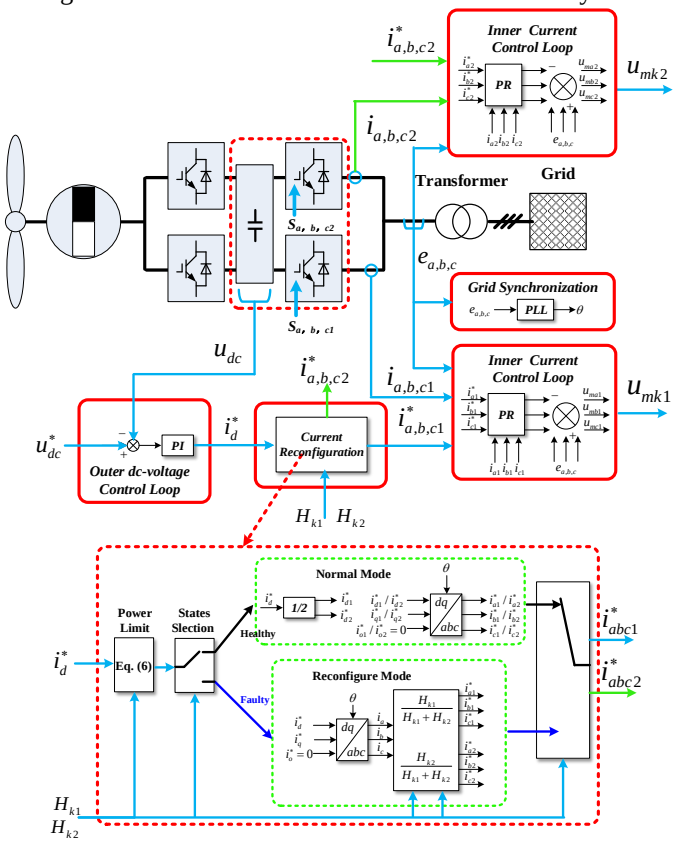

Fig. 6. Reconfigurable control for fault tolerant of parallel wind power converters

V. Simulations

Simulations are performed using Matlab/PLECS to verify the effectiveness of the proposed reconfigurable control strategy. Fig. 6 shows a 3 MW/4 MVA wind power converter made up of two parallel 2 MVA converters. The parameters of a single converter are listed in Table I. The fault conditions of $F_{1\text{-}1d}$ and $F_{2\text{-}2d}$ are verified, whereby, $F_{1\text{-}1d}$, open-circuit fault in leg A_1 and $F_{2\text{-}2d}$, open-circuit faults in A_1 and B_2.

S_{a1} open-circuit fault is considered to verify the influence of current direction on fault detection. Figs. 7 and 8 show the waveforms of fault detection under open-circuit fault at positive and negative current moments, respectively.

TABLE I
Parameters of A Single Converter

Parameter	Value	Unit
Rated Power	1.5	MW
Rated Capacity	2	MVA
DC Link Voltage	1500	V
Output Voltage	690	V
Switching Frequency	2000	Hz
Grid Frequency	50	Hz

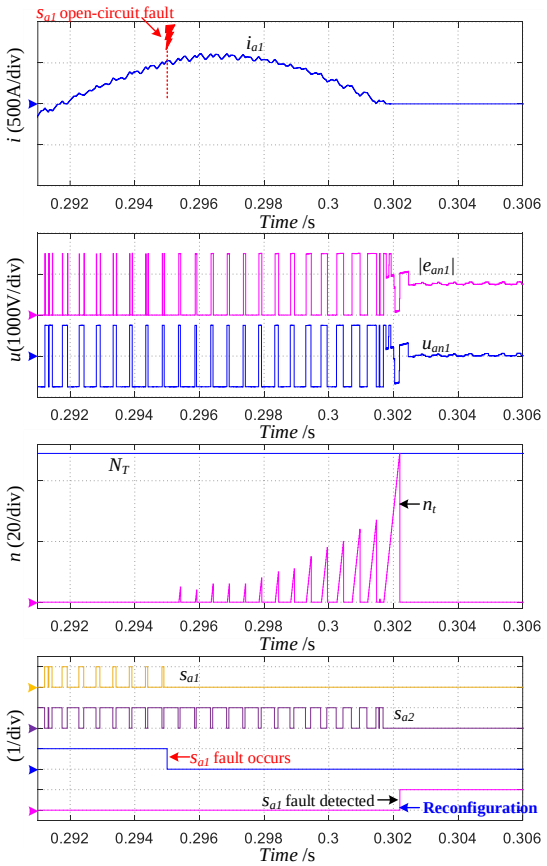

Fig. 7. Fault detection under open-circuit fault at positive current moment

In Fig. 7, S_{a1} open-circuit fault occurs at t=0.295 s, but cannot be detected immediately because the positive current flows through D_{a1}. Although the voltage criterion is satisfied, the time criterion is not satisfied. Only when counter n_t reaches N_T can a fault be detected. Therefore, S_{a1} open-circuit fault cannot be detected until the current turns negative and flows through it at t=0.3022 s. The system switches into reconfiguration mode after the fault is detected.

In Fig. 8, S_{a1} open-circuit fault occurs at t=0.305 s and can be detected immediately because the negative current flows through S_{a1}. Both voltage and time criteria are satisfied.

This article has been accepted for publication in a future issue of this journal, but has not been fully edited. Content may change prior to final publication. Citation information: DOI 10.1109/TSTE.2018.2841018, IEEE Transactions on Sustainable Energy

Counter n_t reaches N_T, and thus, the fault can be detected. Therefore, the fault can be fast detected at t=0.3063 s. The system switches into reconfiguration mode after the fault is detected.

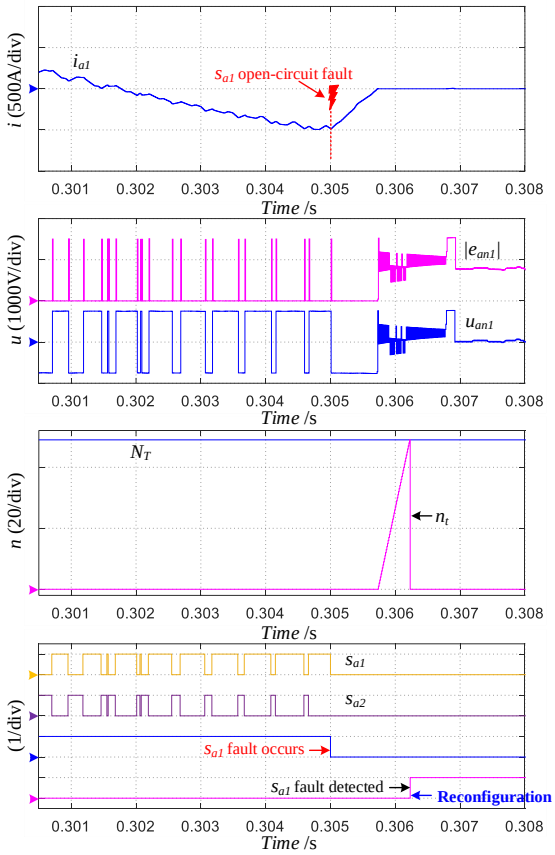

Fig. 8. Fault detection under open-circuit fault at negative current moment

Three operation modes are verified in the simulation, which are defined as follows:

Normal mode: All parallel converters are healthy.

Traditional fault-tolerant mode: Faulty converters are cut off completely and the healthy ones remain in operation.

Reconfiguration mode: Only the faulty legs are cut off and all the healthy legs remain in operation.

Two open-circuit fault types are verified in the simulation, which are $F_{1\text{-}1d}$ occurring at 0.295 s and $F_{2\text{-}2d}$ occurring at 0.355 s. In the simulation, the handling power of system is 1 MW. Figs. 9(*a*) and (*b*) show the simulated results of the three-phase current and phase voltage of each converter with traditional fault-tolerant control and proposed reconfigurable control under $F_{1\text{-}1d}$, respectively. Figs. 10(*a*) and (*b*) show the simulated results of the three-phase current and phase voltage of each converter with traditional fault-tolerant control and proposed reconfigurable control under $F_{2\text{-}2d}$, respectively.

In Fig. 9, S_{a1} open-circuit fault occurs at t=0.295 s. With traditional fault-tolerant control, converter 1 is removed completely post-fault. The parallel system operates in normal mode (0–0.295 s) and traditional fault-tolerant control mode (0.295–0.41 s), as shown in Fig. 9(*a*). The three-phase currents of converter 1 are zero, and that of converter 2 turns to double of the pre-fault values. With the proposed reconfigurable control, only leg A_1 is cut off and legs B_1 and C_1 remain working. The parallel system switches into reconfiguration mode (0.295–0.41s) post-fault, as shown in Fig. 9(*b*). The current of A_2 is double that of the pre-fault after reconfiguration, while other phase currents keep the same as their pre-fault values.

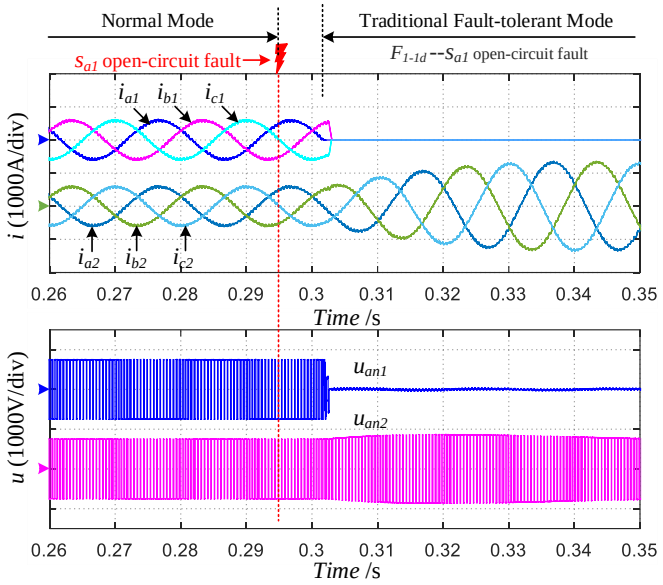

(*a*) with traditional fault-tolerant control

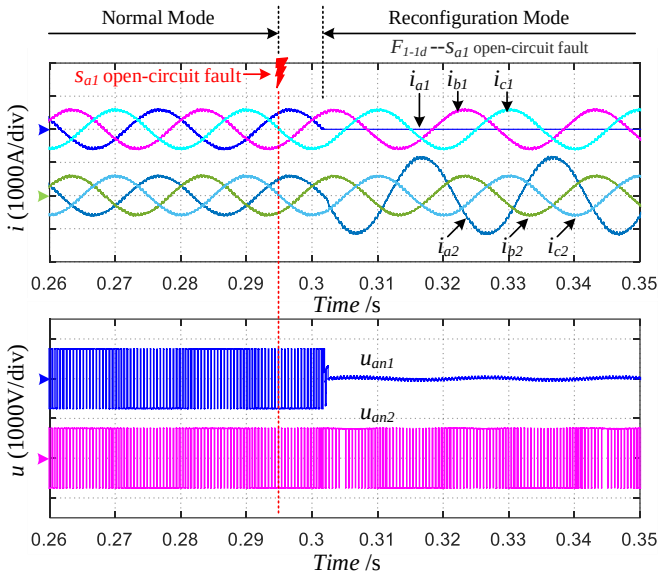

(*b*) with the proposed reconfigurable control

Fig. 9. Three-phase current and phase voltage of each converter under $F_{1\text{-}1d}$

In Fig. 10, S_{b2} open-circuit fault occurs at t=0.355 s. With traditional fault-tolerant control, converter 2 is removed completely post-fault, too. At this time, the parallel power converter system is cut off and the wind turbine has to be shut down. The three-phase currents of converters 1 and 2 both turn to zero post-fault, as shown in Fig. 10(*a*). With the proposed reconfigurable control, only leg B_2 is cut off and legs A_2 and C_2 remain working. The current of B_1 is double that of the pre-fault value, while other phase currents keep the same as their pre-fault values, as shown in Fig. 10(*b*). It is obvious that the proposed reconfigurable control improves the availability of parallel wind power converters and provides multiple-leg fault

This article has been accepted for publication in a future issue of this journal, but has not been fully edited. Content may change prior to final publication. Citation information: DOI 10.1109/TSTE.2018.2841018, IEEE Transactions on Sustainable Energy

ride-through capability to WECS, enhancing its reliability and electricity generation.

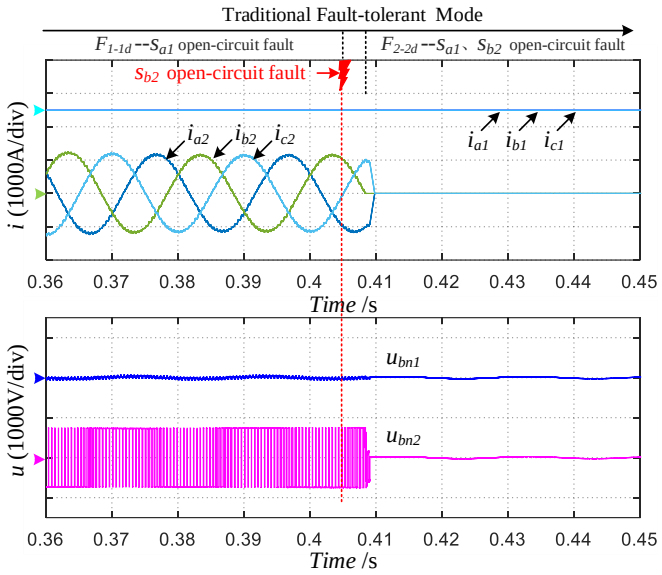

(*a*) with traditional fault-tolerant control

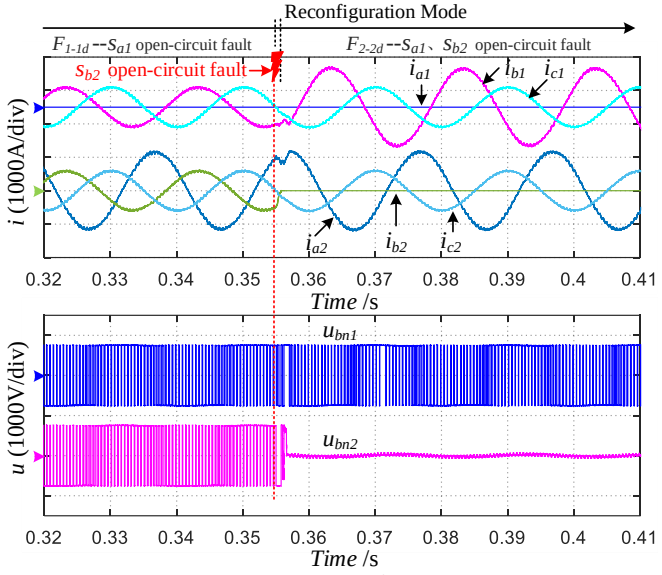

(*b*) with the proposed reconfigurable control

Fig. 10. Three-phase current and phase voltage of each converter under $F_{2\text{-}2d}$

In Figs. 9 and 10, the total post-fault of the three-phase currents of the parallel system remains the same because the total handing power is only 1 MW, which is below 50% of system capacity. However, when the handling power exceeds 50% of system capacity, the system should operate in derating mode. Hence, the handling power of 2 MW pre-fault is considered. Fig. 11 shows the simulated results of the three-phase current and phase voltage of each converter with reconfigurable control under $F_{1\text{-}1d}$, where the system power is 2 MW pre-fault and 1.5 MW post-fault.

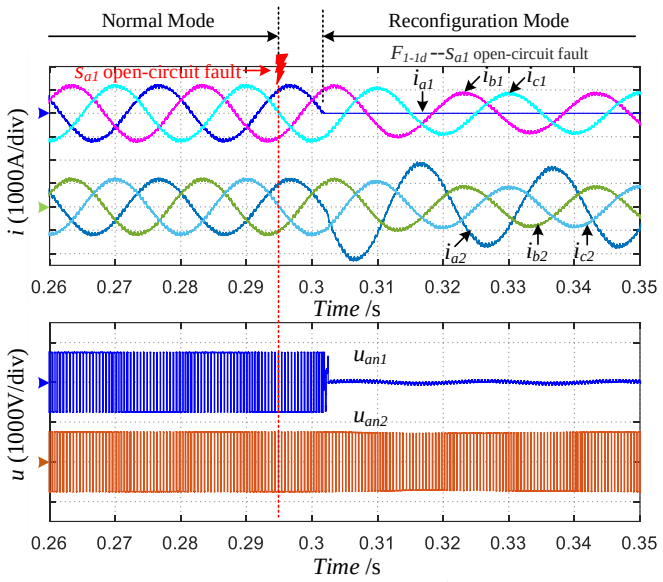

Fig. 11. Three-phase current and phase voltage of each converter with the proposed reconfigurable control under $F_{1\text{-}1d}$

In Fig. 11, S_{a1} open-circuit fault occurs at t=0.295 s. With the proposed reconfigurable control, only leg A_1 is cut off and legs B_1 and C_1 remain working. The parallel system switches into reconfiguration mode post-fault. The system operates in derating mode post-fault. The pre-fault 2 MW is restricted to 1.5 MW post-fault. Therefore, the current of leg A_2 turns smaller than double of the pre-fault value, whereas the currents of all other healthy legs turn smaller than pre-fault after reconfiguration, as shown in Fig. 11.

In Figs. 9 to 11, the dynamic response of the reconfigurable control is fast due to a quick fault detection. Simulation results validate the feasibility and effectiveness of the proposed reconfigurable control. The proposed reconfigurable control only cuts off the faulty legs and makes full use of all healthy legs. This method improves availability of parallel wind power converters and provides multiple-leg faults ride-through capability to WECS.

VI. Experimental Results

The RT-LAB semi-physical experiment is performed to verify the effectiveness of the proposed reconfigurable control strategy. Fig. 12 shows the experimental test setup, which applies a master-slave control. In the master controller, processor OMAP137 is based on an ARM926EJ-S and a TMS320C674x DSP core. The FPGA type is Spartan-6. In the slave controller, the FPGA type is Spartan 3A. The system is made up of two parallel converters. The open-circuit fault conditions of $F_{1\text{-}1d}$ and $F_{2\text{-}2d}$ are verified, in which $F_{1\text{-}1d}$ is an open-circuit fault in leg A_1 and $F_{2\text{-}2d}$ is open-circuit faults in A_1 and B_2. The parameters of a single converter are listed in Table I.

This article has been accepted for publication in a future issue of this journal, but has not been fully edited. Content may change prior to final publication. Citation information: DOI 10.1109/TSTE.2018.2841018, IEEE Transactions on Sustainable Energy

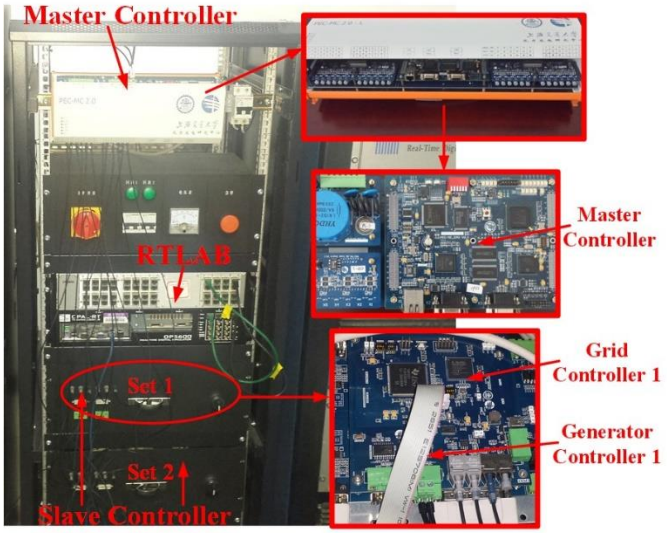

Fig. 12. Experimental test setup

In the experiment, the operating power of parallel system is 1 MW. To validate the circulating current suppressed capability of proposed reconfigurable control, the imbalanced passive components are adopted, that is, the inductance of converter 1 and 2 are set as 0.9 pu and 1 pu, respectively. Figs. 13 shows the experimental results of the currents of phase A and zero sequence circulating current of parallel converters. In Fig.13, without circulating current control, the current difference between legs A_1 and A_2 is serious and the zero sequence circulating current is big. With proposed reconfigurable control, as the currents of legs A_1 and A_2 are controlled to the same reference value separately and accurately, the circulating current can be eliminated. Hence, the zero sequence circulating current can be suppressed effectively.

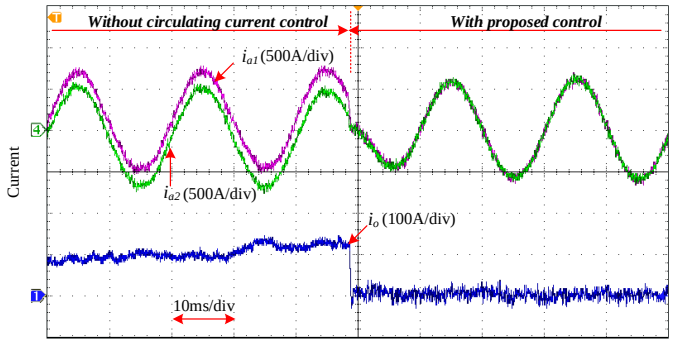

Fig. 13. Waveforms of currents of phase A and zero sequence circulating current of parallel converters.

Figs. 14(*a*) and (*b*) show the experimental results of the currents of parallel converters with traditional fault-tolerant control and the proposed reconfigurable control under $F_{1\text{-}1d}$, respectively. Figs. 15(*a*) and (*b*) show the experimental results of currents of parallel converters with traditional fault-tolerant control and proposed reconfigurable control under $F_{2\text{-}2d}$, respectively.

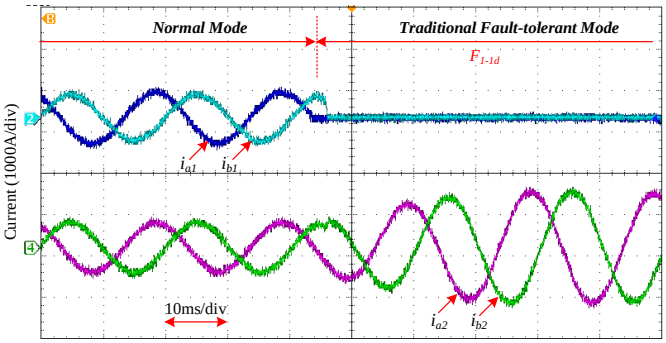

(*a*) with traditional fault-tolerant control

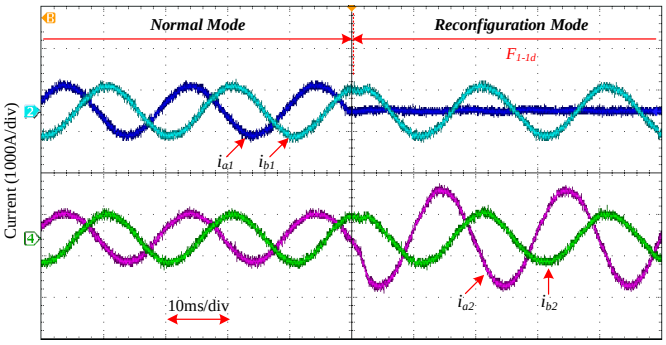

(*b*) with proposed reconfigurable control

Fig. 14. Waveforms of currents of parallel converters pre- and post-fault $F_{1\text{-}1d}$.

In Fig. 14(*a*), converter 1 is removed completely after S_{a1} open-circuit fault occurs with traditional fault-tolerant control and the currents of legs A_1 and B_1 are zero post-fault. The current of converter 2 doubles. By contrast, with the proposed reconfigurable control only leg A_1 is cut off and its current is zero post-fault. The current of leg A_2 is double that of the pre-fault value, while other phase currents keep the same as their pre-fault values, as shown in Fig. 14(*b*).

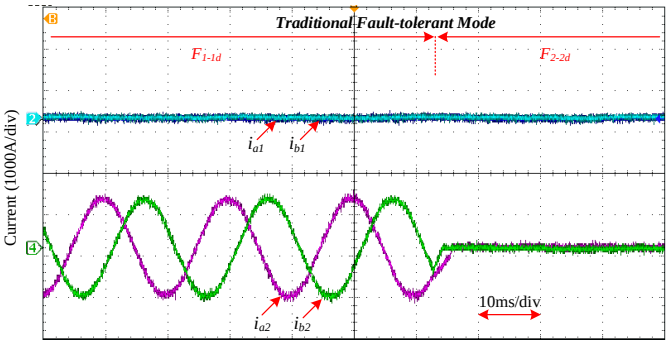

(*a*) with traditional fault-tolerant control

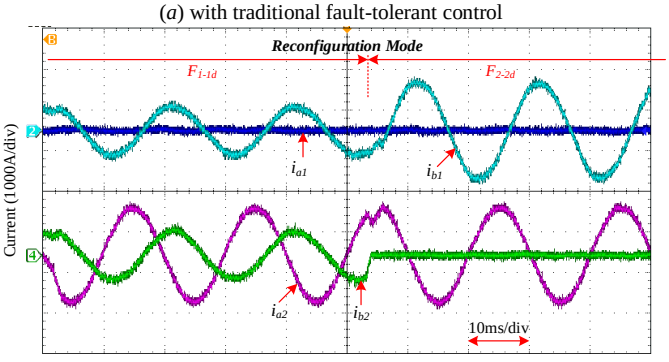

(*b*) with proposed reconfigurable control

Fig. 15. Waveforms of currents of parallel converters pre- and post-fault $F_{2\text{-}2d}$.

This article has been accepted for publication in a future issue of this journal, but has not been fully edited. Content may change prior to final publication. Citation information: DOI 10.1109/TSTE.2018.2841018, IEEE Transactions on Sustainable Energy

In Fig. 15(*a*), with traditional fault-tolerant control, only converter 2 is operating. When S_{b2} open-circuit fault occurs, converter 2 is cut off as well. The current of converter 2 becomes zero post-fault as well. By contrast, with the proposed reconfigurable control, leg B_2 is cut off. The currents of leg B_1 and B_2 turn double and zero, respectively, as shown in Fig. 15(*b*).

Fig. 16 shows experimental results of currents and phase voltages of phase A in parallel converters pre- and post-fault $F_{1\text{-}1d}$. Fig. 17 shows experimental results of currents and phase voltages of phase B in parallel converters pre- and post-fault $F_{2\text{-}2d}$.

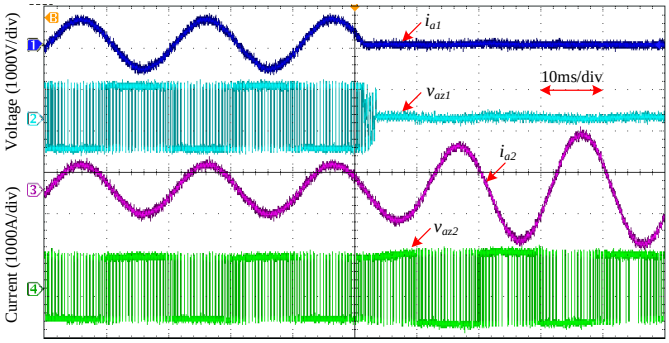

(*a*) with traditional fault-tolerant control

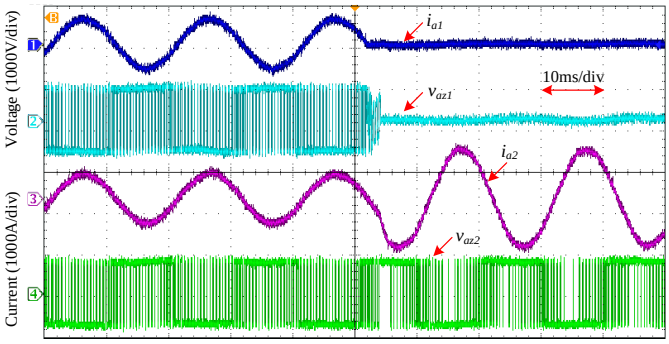

(*b*) with proposed reconfigurable control

Fig. 16. Waveforms of currents and phase voltages of phase A in parallel converters pre- and post-fault $F_{1\text{-}1d}$.

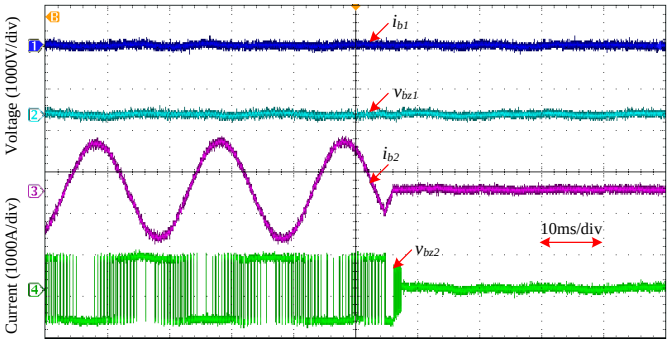

(*a*) with traditional fault-tolerant control

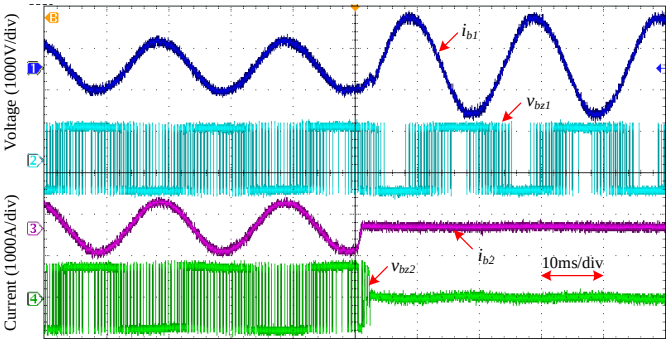

(*b*) with proposed reconfigurable control

Fig. 17. Waveforms of currents and phase voltages of phase B in parallel converters pre- and post-fault $F_{2\text{-}2d}$.

In Figs. 16 and 17, with the proposed reconfigurable control, only faulty legs A_1 and B_2 are cut off. The currents of parallel converters are reconfigured according to their healthy states, which improves the availability of parallel converters and provides multiple-leg fault ride-through capability to the system.

In Figs. 14 to 17, the total post-fault three-phase currents of the parallel system remain the same because the total handing power is only 1 MW, which is below 50% of system capacity. However, when the handling power of the system exceeds 50%, the system should operate in derating mode. So, the handling power of 2 MW is considered. Fig. 18 shows the experimental results of currents of parallel converters with the proposed reconfigurable control under $F_{1\text{-}1d}$. The pre-fault 2 MW is restricted to 1.5 MW post-fault. Therefore, the current of leg A_2 turns smaller than double of the pre-fault value, whereas the currents of all other healthy legs turn smaller than pre-fault after reconfiguration, as shown in Fig. 18.

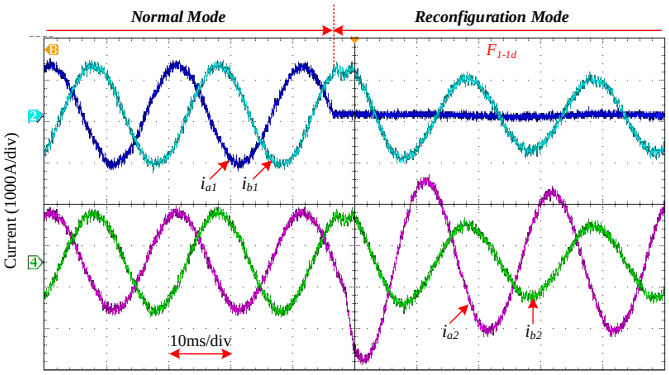

Fig. 18. Waveforms of currents of parallel converters pre- and post-fault $F_{1\text{-}1d}$.

As the wind power converter operates with markedly low rated power over time, the proposed reconfigurable control optimizes control performance and increases generated electricity of the wind turbine and reliability of system under multiple-leg faults. These characteristics are significant in improving economic benefit of wind turbines over time.

VII. Conclusion

A reconfigurable control for fault-tolerant of parallel wind power converters in PMSG WECS is proposed in this paper. The current reference of every phase leg in the parallel converter system is reconfigured post-fault according to their

healthy states. The proposed reconfigurable control is realized in software level, and no redundant hardware is required. Compared with traditional fault-tolerant control, the proposed reconfigurable control fully uses of all healthy legs by only cutting off faulty legs rather than the faulty converter. The reconfigurable control improves availability of parallel wind power converters and provides multiple-leg faults ride-through capability to WECS, enhancing its reliability and electricity generation. The simulation and experimental results validate the feasibility and effectiveness of the proposed reconfigurable control, which has practical significances in various field applications.

REFERENCES

[1] H. Polinder, J. A. Ferreira, B. B. Jensen, A. B. Abrahamsen, K. Atallah, and R. A. McMahon, "Trends in Wind Turbine Generator Systems," *IEEE J. of Emerg. Sel. Topics Power Electron.*, vol.1, no.3 pp. 174-185, Sep. 2013.

[2] F. Blaabjerg, M. Liserre and K. Ma, "Power Electronics Converters for Wind Turbine Systems," *IEEE Trans. Ind. Appl.*, vol. 48, no.2, pp. 708-719, Mar./Apr. 2012.

[3] J. Wang, R. Qu, Y. Tang, Y. Liu, B. Zhang, J. He, Z. Zhu, H. Fang, and L. Su, "Design of a Superconducting Synchronous Generator With LTS Field Windings for 12 MW Offshore Direct-Drive Wind Turbines," *IEEE Trans. Ind. Electron.*, vol. 63, no.3, pp. 1618-1628, Mar. 2016.

[4] M. Liserre, R. Cardenas, M. Molinas, and J. Rodriguez, "Overview of Multi-MW Wind Turbines and Wind Parks," *IEEE Trans. Ind. Electron.*, vol. 58, no.4, pp. 1081-1095, Apr. 2011.

[5] B. Singh, V. Emmoji, and S. Singh, "Performance evaluation of series and parallel connected grid side converters of DFIG," in *Proc. IEEE Power and Energy Soc. General Meeting*, Jul. 2008, pp.1–8.

[6] K. E. Okedu, ''Enhancing DFIG wind turbine during three-phase fault using parallel interleaved converters and dynamic resistor,'' *IET Renew. Power Generat.*, vol. 10, no. 8, pp. 1211–1219, Sep. 2016.

[7] R. Li and D. Xu, "Parallel Operation of Full Power Converters in Permanent-Magnet Direct-Drive Wind Power Generation System," *IEEE Trans. Ind. Electron.*, vol. 60, no.4, pp. 1619-1629, Apr. 2013.

[8] Xu Z, Li R, Zhu H, et al. "Control of parallel multiple converters for direct-drive permanent-magnet wind power generation systems," *IEEE Trans. Power Electron.*, vol.27, no.3, pp. 1259-1270, Mar. 2012.

[9] D. Zhou, F. Blaabjerg, T. Franke, M. Tonnes, and M. Lau, "Comparison of Wind Power Converter Reliability With Low-Speed and Medium-Speed Permanent-Magnet Synchronous Generators," *IEEE Trans. Ind. Electron.*, vol. 62, no. 10, pp. 6575-6584, Oct. 2015.

[10] A. Isidoril, F. M. Rossi, F. Blaabjerg, and K. Ma, "Thermal Loading and Reliability of 10-MW Multilevel Wind Power Converter at Different Wind Roughness Classes," *IEEE Trans. Ind. Appl.*, vol.50, no.1, pp. 484-494, Jan./Feb. 2014.

[11] Carroll J, McDonald A, McMillan D. "Reliability comparison of wind turbines with DFIG and PMG drive trains," *IEEE Trans. Energy Convers.*, vol.30, no.2, pp. 663-670, Jun. 2015.

[12] X. Kaigui, J. Zefu and L. Wenyuan, "Effect of wind speed on wind turbine power converter reliability," *IEEE Trans. Energy Convers.*, vol. 27, no.1, pp. 96-104, Mar. 2012.

[13] Fischer K, Stalin T, Ramberg H, et al. "Field-experience based root-cause analysis of power-converter failure in wind turbines," *IEEE Trans. Power Electron.*, vol.30, no.5, pp,2481-2492, May 2015.

[14] Yang S, Bryant A, Mawby P, et al. "An industry-based survey of reliability in power electronic converters," *IEEE Trans. Ind. Appl.*, vol.47, no.3, pp. 1441-1451. May/Jun. 2011.

[15] B. M. H. Jassim, D. J. Atkinson and B. Zahawi, "Modular Current Sharing Control Scheme for Parallel-Connected Converters," *IEEE Trans. Ind. Electron.*, vol. 62, no.2, pp. 887-897, Feb. 2015.

[16] X. Zhang, T. Wang, X. Wang, G. Wang, Z. Chen, and D. Xu, "A Coordinate Control Strategy for Circulating Current Suppression in Multiparalleled Three-Phase Inverters," *IEEE Trans. Ind. Electron.*, vol. 64, no.1, pp. 838-847, Jan. 2017.

[17] X. Yu and A. M. Khambadkone, "Reliability Analysis and Cost Optimization of Parallel-Inverter System," *IEEE Trans. Ind. Electron.*, vol. 59, no.10, pp. 3881-3889, Oct. 2012.

[18] Wang H, Zhou D, Blaabjerg F. "A reliability-oriented design method for power electronic converters,", in *Proc. 28th Appl. Power Electron. Conf. Exp*., Mar. 2013, pp. 2921-2928.

[19] Chen G, Zhang J, Zhu M, et al. "Adaptive thermal control for power fluctuation to improve lifetime of IGBTs in multi-MW medium voltage wind power converter," in *Proc. Int. Power Electron. Conf.*, May 2014, pp. 1496-1500.

[20] Zhou D, Blaabjerg F, Lau M, et al. "Optimized reactive power flow of DFIG power converters for better reliability performance considering grid codes," *IEEE Trans. Ind. Electron.*, vol.62, no.3, pp. 1552-1562, Mar. 2015.

[21] T. Lei, M. Barnes, S. Smith, S. Hur, A. Stock, and W. E. Leithead, "Using Improved Power Electronics Modeling and Turbine Control to Improve Wind Turbine Reliability," *IEEE Trans. Energy Convers.*, vol. 30, no.3, pp. 1043-1051, Sep. 2015.

[22] W. Zhang, D. Xu, P. N. Enjeti, H. Li, J. T. Hawke, and H. S. Krishnamoorthy, "Survey on Fault-Tolerant Techniques for Power Electronic Converters," *IEEE Trans. Power Electron.*, vol. 29, no.12, pp. 6319-6331, Dec. 2014.

[23] B. Mirafzal, "Survey of Fault-Tolerance Techniques for Three-Phase Voltage Source Inverters," *IEEE Trans. Ind. Electron.*, vol. 61, no.10, pp. 5192-5202, Oct. 2014.

[24] Q. Chen, G. Liu, W. Zhao, L. Qu, and G. Xu, "Asymmetrical SVPWM Fault-Tolerant Control of Five-Phase PM Brushless Motors," *IEEE Trans. Energy Convers.*, vol. 32, no.1, pp. 12-22, Mar. 2017.

[25] G. Scarcella, G. Scelba, M. Pulvirenti, and R. D. Lorenz, "Fault-Tolerant Capability of Deadbeat-Direct Torque and Flux Control for Three-Phase PMSM Drives," *IEEE Trans. Ind. Appl.*, vol. 53, no.6, pp. 5496-5508, Nov./Dec. 2017.

[26] I. Gonzalez-Prieto, M. J. Duran, H. S. Che, E. Levi, M. Bermudez, and F. Barrero, "Fault-Tolerant Operation of Six-Phase Energy Conversion Systems With Parallel Machine-Side Converters," *IEEE Trans. Power Electron.*, vol. 31, no.4, pp. 3068-3079, Apr.2016.

[27] Z. Wang, J. Chen, M. Cheng, and Y. Zheng, "Fault-Tolerant Control of Paralleled-Voltage-Source-Inverter-Fed PMSM Drives," *IEEE Trans. Ind. Electron.*, vol. 62, no.8, pp. 4749-4760, Aug. 2015.

[28] W. Zheng, C. Jian and C. Ming, "Fault tolerant control of double-stator-winding PMSM for open phase operation based on asymmetric current injection,", in *Proc. 17th Int. Conf. Electr. Machines Sys.*, Oct. 2014, pp. 3424-3430.

[29] J. Lee and K. Lee, "Open-Switch Fault Tolerance Control for a Three-Level NPC/T-Type Rectifier in Wind Turbine Systems," *IEEE Trans. Ind. Electron.*, vol. 62, no.2, pp. 1012-1021, Feb. 2015.

[30] W. Wang, M. Cheng, B. Zhang, Y. Zhu, and S. Ding, "A Fault-Tolerant Permanent-Magnet Traction Module for Subway Applications," *IEEE Trans. Power Electron.*, vol. 29, no.4, pp. 1646-1658, Apr. 2014.

[31] M. Merai, W. Naouar, I. Slama-Belkhodja, and E. Monmasson, "FPGA-Based Fault Tolerant Space Vector Hysteresis Current Control for Three-Phase Grid Connected Converter," *IEEE Transa. Ind. Electron.*, vol. 63, no.11, pp.7008-7017. Nov. 2016.

[32] Nguyen T D, Tuong N D, Lee H H. "Carrier-based PWM strategy for post-fault reconfigured 3-level NPC inverter under imbalanced dc-link voltages," in *Proc. 8th Int. Power Electron. Motion Control Conf*., Jun.2016, pp. 2406-2411.

[33] M. SHAHBAZI, P. POURE, S. Saadate, and M. Zolghadri, "FPGA-based reconfigurable control for fault-tolerant back-to-back converter without redundancy," *IEEE Trans. Ind. Electron.*, vol.60, no.8, pp.3360-3371, Aug. 2012.

[34] Karimi S, Gaillard A, Poure P,et al. "FPGA-Based Real-Time Power Converter Failure Diagnosis for Wind Energy Conversion Systems," *IEEE Trans. Ind. Electron.*, vol.55, no.12, pp. 4299-4308, Dec. 2008.

[35] Caseiro L M A, Mendes A M S. "Real-Time IGBT Open-Circuit Fault Diagnosis in Three-Level Neutral-Point-Clamped Voltage-Source Rectifiers Based on Instant Voltage Error," *IEEE Trans. Ind. Electron.*, vol.62, no.3, pp. 1669-1678, Mar. 2015.

[36] Genduso F, Cecati C, Di Tommaso A O,et al, "Comprehensive Modelling and and Experimental Testing of Fault Detection and Management of a Non-Redundant Fault-Tolerant VSI," *IEEE Trans. Ind. Electron.*, vol.62, no.3, pp. 3945-3954, Mar. 2015.

[37] Q.-T. An, L.-Z. Sun, K. Zhao, and L. Sun, "Switching function model based fast diagnostic method of open-switch faults in inverters without sensors," *IEEE Trans. Power Electron.*, vol. 26, no. 1, pp. 119–126, Jan. 2011.

[38] C. Citro, P. Siano and C. Cecati, "Designing Inverters' Current Controllers With Resonance Frequencies Cancellation," *IEEE Trans. Ind. Electron.*, vol. 63, no.5, pp. 3072-3080, May 2016.

Gen Chen (S'13) received the B.E. degree in electrical engineering from the China University of Mining Technology, Xuzhou, China, in 2011. He is currently pursuing the Ph.D. degree with Department of Electrical Engineering, Shanghai Jiao Tong University, Shanghai, China.

His research interests include the reliability of high power wind power converter, fault tolerant control of power converter, digital drive of high power IGBT.

Xu Cai received the B.E. degree in electrical engineering from the Southeast University, Nanjing, China, in 1983 and the M.S. and Ph.D. degrees in electrical engineering from the China University of Mining and Technology, in 1988 and 2000, respectively.

From 1989 to 2001, he was an Associate Professor with the Department of Electrical Engineering, China University of Mining and Technology. Since 2002, he has been a Professor with the Department of Electrical Engineering, Shanghai Jiao Tong University, where he has been the Director of the Wind Power Research Center, Shanghai Jiao Tong University, since 2008.

His special fields of interests lie in power electronics and renewable energy exploitation and utilization.

Corresponding author: (xucai@sjtu.edu.cn).